Spray-Coating Route for Highly Aligned and Large-Scale Arrays of Nanowires

Ossama Assad,[†] Alexander M. Leshansky,[†] Bin Wang,[†] Thomas Stelzner,[‡] Silke Christiansen,[‡,§] and Hossam Haick[†,*]

[†]The Department of Chemical Engineering and Russell Berrie Nanotechnology Institute, Technion—Israel Institute of Technology, Haifa 32000, Israel, [‡]Institute of Photonic Technology e.V., Albert-Einstein-Straße 9, 07745 Jena, Germany, and [§]Max-Planck-Institute for the Science of Light, Günther-Scharowsky-Straße 1, 91058 Erlangen, Germany

ABSTRACT Technological implementation of nanowires (NWs) requires these components to be organized with controlled orientation and density on various substrates. Here, we report on a simple and efficient route for the deposition of highly ordered and highly aligned NW arrays on a wide range of receiver substrates, including silicon, glass, metals, and flexible plastics with controlled density. The deposition approach is based on spray-coating of a NW suspension under controlled conditions of the nozzle flow rate, droplet size of the sprayed NWs suspension, spray angle, and the temperature of the receiver substrate. The dynamics of droplet generation is understood by a combined action of shear forces and capillary forces. Provided that the size of the generated droplet is comparable to the length of the single NW, the shear-driven elongation of the droplets results presumably in the alignment of the confined NW in the spraying direction. Flattening the droplets upon their impact with the substrate yields fast immobilization of the spray-aligned NWs on the surface due to van der Waals attraction. The availability of the spray-coating technique in the current microelectronics technology would ensure immediate implementation in production lines, with minimal changes in the fabrication design and/or auxiliary tools used for this purpose.

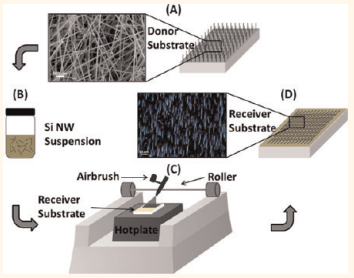

KEYWORDS: silicon · silver · GaN · nanowire · array · spray-coating · deposition

The ability of individual nanowires (NWs) to carry electrical current makes them promising building blocks in various nanoelectronic device concepts. Individual NWs have been used to assemble a range of nanoscale devices, including p–n diodes,[1–3] bipolar junction transistors,[4] field effect transistors,[3–9] electrochemical devices,[10–12] biochemical sensors,[5,6,13–24] optoelectronic devices,[25–30] and more. Nevertheless, there are still many challenges in creating such devices: (i) difficulties in connecting the individual NW to the macroscopic world, although significant progress has been made in this field; (ii) fluctuations in the position of NWs between adjacent metallic electrodes; (iii) understanding the mode of power dissipation when NWs are used as devices or in devices; and (iv) maintaining high signal-to-noise ratio in complex nanodevices. For technological applications, the ease and effectiveness with which NWs are assembled and integrated into large-scale devices are of critical importance.

An alternative approach to the individual NW-based devices[31–44] is the application of a platform in which NW arrays are used to exploit their specific properties (*e.g.*, large surface-to-volume ratio), but which do not require highly sophisticated fabrication techniques.[31–44] This approach is based on controlling deposition properties of NWs, yielding synergetic combinations of the nanoscale and the macroscale worlds. These NW arrays circumvent the requirement of position and structural control because the devices display the average properties of many distributed NWs. The NW arrays could be processed into devices of varying sizes using conventional microfabrication technology, characterized by high stability, repeatability, and better error tolerance.[31–44]

Arrays of NWs can be achieved either by top-down or bottom-up fabrication techniques. The top-down approach depends heavily on multistep (e-beam) lithography and lift-off techniques, which are serial, time-consuming, and expensive. The bottom-up approach relies on the transfer of NWs from the growth chip to a suitable substrate. This includes, but is not confined to, the following:

- Flow-assisted alignment: this approach incorporates microfluidic channels to enable directional flow and deposition of a NW suspension on a solid-state surface.[24,25]
- Deposition by chemical interactions: this approach relies on the interactions between the NWs and the receiver substrate. The deposition sites strongly depend on the surface chemical functionality.[44]

* Address correspondence to hhossam@technion.ac.il.

Received for review November 20, 2011 and accepted May 3, 2012.

Published online May 03, 2012
10.1021/nn204513y

- Langmuir–Blodgett technique: this approach uses a surfactant to generate an aligned NW layer on a surface of liquid, from where the NW layer is transferred to a planar substrate.[33–35]
- Blown-bubble technique: this approach involves expansion of a polymer suspension of NWs to form a bubble that can be transferred to a substrate.[36]
- Electric field directed deposition: this approach relies on alternating voltage between adjacent electrodes to polarize and align the NWs before deposition on a solid substrate.[37–39]
- Contact transfer technique: this approach uses a shear force generated by mechanical sliding of two solid surfaces with respect to one other, where one surface is the NW growth substrate and the other is the device.[40–43]

In this paper, we report on a simple and efficient method for the deposition of highly ordered and aligned NW arrays on a wide range of receiver substrates, including silicon, glass, metals, and flexible plastics with controlled density. The reported deposition method is based on a spray-coating process under controlled conditions of the nozzle flow, droplet size, spray-coating angle, and temperature of the receiver substrate. The deposition and alignment mechanism of the spray-coated NWs is discussed with the help of appropriate experimental findings. Representative application of these films is reported. The cost-effectiveness of the spray-coating technique has a potential for immediate implementation in the industry and/or line productions.

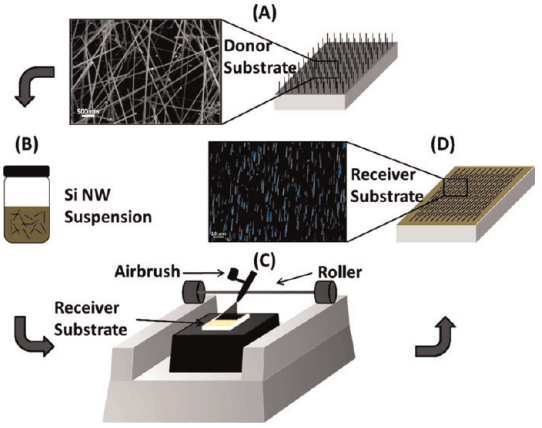

Figure 1. Schematic of the spray-coating process that involves a direct transfer of NW suspension to the receiver substrates. (A) Schematic and scanning electron microscopy (SEM) image of the NW sample used in this study. (B) Schematic of the NW suspension. (C) Schematic of the assembled apparatus used in this study. (D) Schematic and optical microscopy image of Si NW spray-coated on the SiO_x/Si substrate.

RESULTS

The deposition method developed and tested in the current study is based on a spray-coating process under controlled conditions (Figure 1). The spray-coating system consisted of a hot plate for controlling the temperature of the receiver substrate, a pressure-flow spray nozzle module, a nozzle movement module, a nozzle angle control module, and a nozzle cross-section control module. The spray-coating setup was designed considering the NW suspension viscosity, the spray nozzle, the NW suspension supply, and other process variables; see the Methods section. Using this setup, a series of systematic experiments were carried out to determine and to understand the main factors controlling the alignment and average density of the deposited NWs. In the current study, a NW is considered misaligned if its axis forms an angle of >10° with respect to the spray direction.

Effect of Operational Parameters on the Deposited NWs. Unless otherwise stated, the main presentation and discussion of the spray-coating approach will be focused on Si NWs. Figure 2A shows the effect of the carrier gas flow on the alignment of Si NWs by introducing various carrier gas (nitrogen) pressures into the spray gun: 5, 10, 20, 30, 40, 50, and 60 psi. The results show that the higher the carrier gas pressure in the 5–20 psi range, the higher the alignment of the Si NWs with respect to the flow direction. The highest

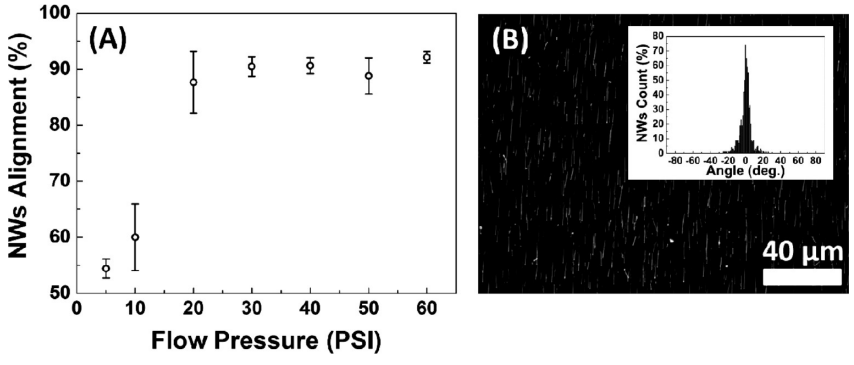

Figure 2. (A) The percentage of the aligned Si NWs at various spray flow pressures: 5, 10, 20, 30, 40, 50, and 60 psi. Each point in the figure was obtained by a statistical analysis of ~200 Si NWs. (B) Representative dark-field optical image of spray-coated Si NWs at 40 psi spray flow pressure and the constituent statistical analysis of 700 Si NWs with respect to the flow direction. The spray-coating process was carried out on a SiO_x/Si receiver substrate at 75 °C.

alignment was obtained at 20−60 psi gas pressure. In this region, the average alignment ranged between 87.7% and 92.2%. However, the smallest variances in the Si NW alignment were obtained at 30, 40, and 60 psi. Since 30 and 40 psi means lower operation costs than 60 psi, they could be considered as the optimal gas pressure values for the Si NW spray-coating process. Figure 2B shows a representative optical (dark field) image and angle distribution histogram of spray-coated Si NWs on a SiO_x/Si substrate at optimal gas pressure (40 psi). As seen in the figure, more than 90% of the Si NWs were aligned within ±10° of the flow direction. The rest were distributed between *ca.* −30° and +30° with respect to the flow direction.

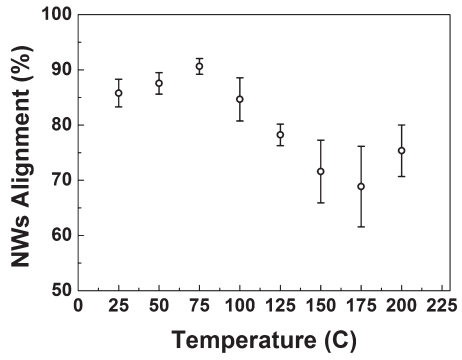

Figure 3. Percentage of the aligned Si NWs *versus* the temperature of the receiver substrate. The spray-coating process was carried out on a SiO_x/Si receiver substrate with a spray flow pressure of 40 psi. Each point in the figure was obtained by statistical analysis of ~200 Si NWs.

Figure 3 shows the alignment degree of Si NWs when sprayed with constant (40 psi) spray flow pressure on SiO_x/Si substrates at various temperatures (25−200 °C). As seen in the figure, increasing the temperature of the receiver substrate from 25 °C to a temperature that is close to the boiling point of the suspension's solvent (2-propanol; $T_{boiling}$ ~82 °C) increased the average alignment of the Si NWs, increased the reproducibility from sample to sample, and decreased the obtained variance. Representative alignments under these conditions include 85.8 ± 2.5% at 25 °C and 90.6 ± 1.4% at ~75 °C. Increasing the temperature of the receiver substrate above ~80 °C decreased the alignment degree of the Si NWs from 90.6 ± 1.4% at ~75 °C to 68.9 ± 7.3% at ~175 °C and to 75.4 ± 4.7% at ~200 °C. Additionally, increasing the temperature of the receiver substrate above ~80 °C decreased the reproducibility from sample to sample by 3−5 times, compared to the equivalent value obtained at ~75 °C.

Controlling the concentration of the Si NW suspension and/or the flow duration affected the density of the deposited Si NWs. The higher the spray-coating duration time, the higher the density of the deposited Si NWs (see Figure 4). For example, a 60 s flow duration produced a density of 200 Si NW per 100 μm, with an average NW−NW separation of ~500 nm

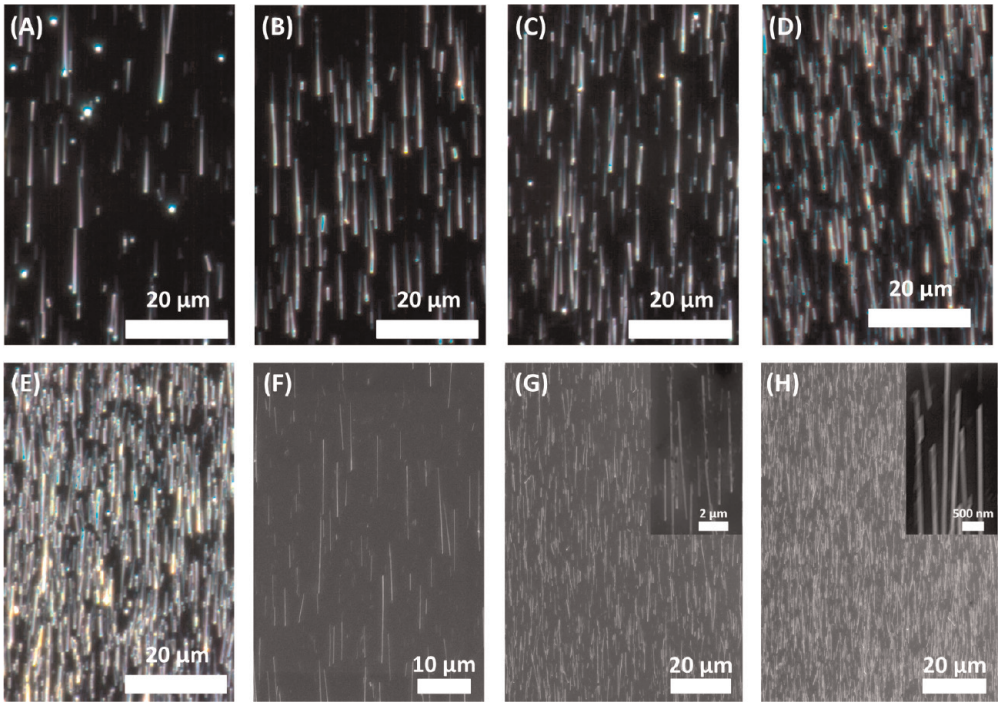

Figure 4. Optical microscopy images of Si NWs aligned by spray flow for different durations: (A) 5 s; (B) 10 s; (C) 20 s; (D) 30 s; and (E) 60 s. Scanning electron microscopy (SEM) image of Si NWs aligned by spray flow for different durations: (F) 30 s; (G) 60 s; and (H) 90 s. All experiments were carried out with an air pressure of 40 psi and on a receiver substrate at 75 °C. The maximum area coverage by a nozzle with an air pressure of 40 psi, 5° between the spray gun and the receiver substrate, and 75 °C for the receiver substrate was 50 mm^2.

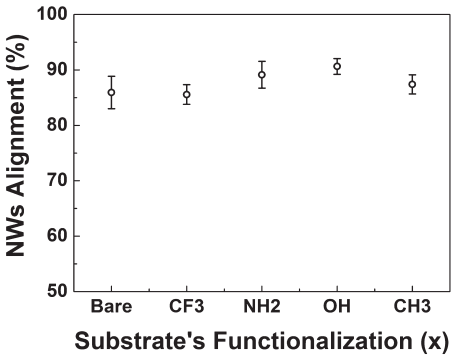

Figure 5. Percentage of the aligned Si NWs at various functionalization of the SiO_x/Si receiver substrate. The bare substrate corresponds to untreated substrate. The $-OH$ functional groups were obtained by treating the SiO_x/Si substrate with oxygen plasma for 30 min. The $-CH_3$, $-NH_2$, and $-CF_3$ functional groups were obtained by self-assembly of trichlorooctadecylsilane, 3-aminopropyltrimethoxysilane, and 2-perfluorooctylethyltrichlorosilane on the SiO_x/Si substrate, respectively. The spray-coating process was carried out on a SiO_x/Si receiver substrate at 75 °C with a spray flow pressure of 40 psi. Each point in the figure was obtained by statistical analysis of ~200 Si NWs.

(see Figure 4G). Extended deposition time (~90 s) produced Si NW arrays with (reduced) spacing on the order of 200 nm (see Figure 4H). This control over the density of the deposited Si NWs, while leaving the alignment of the Si NWs unaffected, was similar to other advanced techniques, such as flow-assisted alignment,[24,25] blown-bubble technique,[36] and contact transfer technique.[40−43] However, the cost-effectiveness of the spray-coating technique has the advantage of immediate implementation in the industry.

The compatibility of the spray-coating process with the substrate type and dimensions was examined in four major levels. In the first level of this examination, the alignment of the spray-coated Si NWs was examined with respect to the surface modification of the receiver substrate: (i) bare SiO_x/Si surface; (ii) CH_3-terminated surface; (iii) CF_3-terminated surface, which has high hydrophobicity and minimal "sticky" and/or "adhesive" characteristics with regard to the deposited Si NWs; (iv) OH-terminated surface; and (v) NH_2-terminated surface, which is known to have high bonding and/or interactions with the deposited Si NWs. As seen in Figure 5, optimized spray-coating conditions (40 psi flow gas pressure and a receiver substrate at 75 °C) allowed high alignment (86−91%) of the deposited Si NWs, irrespective of the surface modification type.[45] In the second level of this examination, Si NWs were spray coated on a wide range of rigid (silicon, glass, and metal) substrates and flexible substrates. As seen in Figure 6, optimized spray-coating conditions allowed high alignment of the deposited Si NWs on both the rigid substrates and flexible plastic substrates, which can subsequently be bent into curved structures (see Figure 6A). In the third level of this examination, the

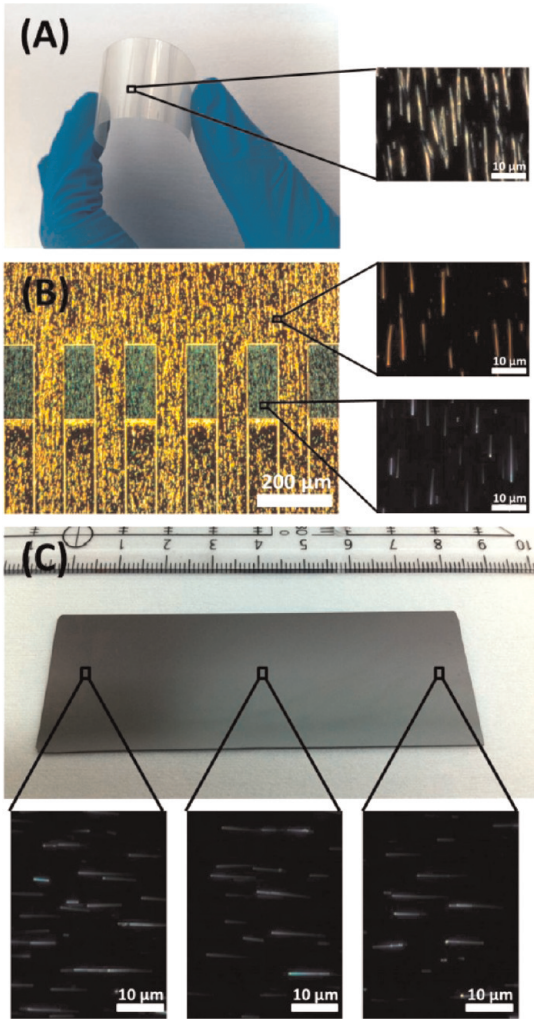

Figure 6. (A) Image of spray-coated Si NWs on a plastic substrate. Inset: Dark-field optical image showing the Si NWs found in the marked area. (B) Image of Si NWs spray-coated on predefined Ti/Au (20/200 nm) patterns (100 μm width × 200 μm length) on a SiO_x/Si substrate. Inset: Dark-field optical image showing the Si NWs found in the marked metal and SiO_x/Si locations. (C) Image of Si NWs spray-coated on 80 mm SiO_x/Si wafer and its line-scanning alignment analysis. Insets: High-resolution dark-field images highlighting the alignment of Si NWs in the marked locations.

spray-coating technique was examined on substrates having predefined patterns. Figure 6B shows a Ti/Au (20/200 nm) patterns (100 μm width × 200 μm length) on a SiO_x/Si substrate. Following the spray-coating, Si NWs were successfully transferred on the metal layer as well as in the openings between the adjacent metallic areas with good orientation alignment. A subsequent lift-off process results in the removal of the metal while leaving behind only Si NWs that were assembled in the opened regions. To achieve finer spatial resolution, electron-beam lithography should be used to define the pattern openings. In the fourth phase of this examination, spray-coating of Si NWs was attempted on large-area substrates. Figure 6C shows that the alignment and density of the deposited Si NWs were

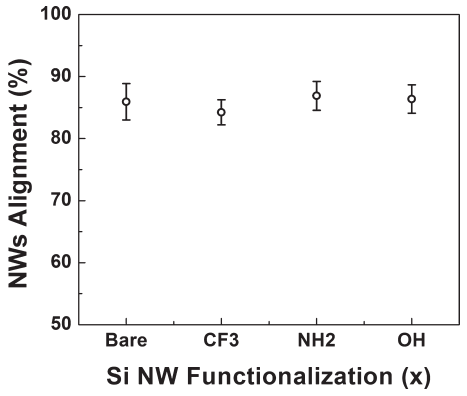

Figure 7. NW alignment as a function of the surface functionalization of the Si NWs. Bare Si NWs correspond to the use of untreated Si NWs; The −OH corresponds to Si NWs that were treated with oxygen plasma for 1 min; the $-NH_2$ corresponds to Si NWs that were treated with aminopropyltrimethoxysilane; and the $-CF_3$ corresponds to Si NWs that were treated with 2-perfluorooctylethyltrichlorosilane. The spray-coating process was carried out on a SiO_x/Si receiver substrate with a spray flow pressure of 40 psi and at a receiver substrate at 75 °C. Each point in the figure was obtained by statistical analysis of ∼200 Si NWs.

remarkably uniform, irrespective of the coordination/location on the wafer's surface. Statistical analysis over more than ∼500 Si NWs in different locations over the entire substrate showed that more than 85% of the Si NWs are aligned within 10° of the flow direction.

The widespread characteristics of the spray-coating approach were explored in three levels of examination. In the first level of this examination, the alignment of the spray-coated Si NWs was probed with respect to the surface modification of the Si NWs (Figure 7): (i) bare Si NWs; (ii) CF_3-terminated Si NWs; (iii) OH-terminated Si NWs; and (iv) NH_2-terminated Si NWs. As seen in Figure 7, optimized spray-coating conditions (40 psi flow gas pressure and 75 °C receiver substrate) allowed high alignment (84−87%) of the deposited Si NWs with respect to the flow direction, irrespective of the surface modification type.[45] In the second level of this examination, the alignment of the spray-coated Si NWs was examined with respect to the Si NW length. A stable suspension of ∼2 μm Si NWs, approximately 6 times shorter than the Si NWs (∼12 μm) used in our studies, was suspended in 2-propanol. Optimized spray-coating conditions allowed high alignment (84%) of the deposited Si NWs with respect to the flow direction. In the third level of this examination, stable suspensions of GaN NWs or Ag NWs in 2-propanol were prepared; see Methods section. The sprayed GaN NWs and Ag NWs were successfully transferred to the receiver substrate (40 psi flow gas pressure and 75 °C receiver substrate) with good orientation alignment. Statistical analysis of more than ∼100 GaN NWs and more than ∼100 Ag NWs showed that >86% of the GaN NWs and Ag NWs were aligned within 10° of the flow direction (see Supporting Information, Figure 1S). Higher alignment degree of the GaN NWs and Ag NWs could be expected upon optimizing the concentration and length uniformity of the NWs in the sprayed suspension and, also, upon optimizing the spray-coating parameters (temperature of the receiver substrate, flow rate, flow direction, *etc.*). Altogether, these results demonstrate that the spray-coating technique is compatible with a wide range of NWs, irrespective of their surface properties and/or size.

Spray-Coated Si NWs in Field Effect Transistors. The high degree of alignment and controlled density of (Si) NWs is important in a number of integrated electronic devices as well as in their constituent applications. To illustrate this potential, Si NWs were spray-coated on a 300 nm thermal oxide coated heavily doped p-type silicon wafer. The deposited Si NWs were then configured as back-gated field-effect transistors (FETs) by defining Ti/Au (40/110 nm) source (S) and drain (D) contacts with a channel length[46] of 2 μm and a channel width ranging from 1 μm up to 350 μm. The density of the connected Si NWs between the source and drain electrodes was similar for all channel widths (∼1 NW/μm^2). This density has been found by Li *et al.*[47] to provide optimal performance and minimum variability across the device.

Figure 8A shows the drain current (I_{ds}) *versus* drain−source voltage (V_{ds}) curves of spray-coated Si NW arrays (∼20 Si NWs) by utilizing a sweeping voltage range from 0 to +2 V at various gate voltages (V_{gs}). As seen in the figure, the $I_{ds}-V_{ds}$ curves exhibited a typical accumulation mode of p-channel transistor behavior. The plot of I_{ds} *versus* V_{gs} (see Figure 8B) at a constant $V_{ds} = +2$ V exhibited a small current when the V_{gs} was more positive than the threshold voltage (V_{th}). The I_{ds} increased linearly with increasing V_{gs} in the negative direction and provided $V_{th} = 4.15$ V. The slope in the linear region of the I_{ds} *versus* V_{gs} gave a transconductance, $g_m = dI_{ds}/dV_{gs}$, of 0.013 μS at $V_{ds} = 2$ V. The on-currents (I_{on}) of these devices were as high as 0.55 μA, and the on−off current ratio was nearly 10^5. The electrical features of the Si NW FETs were satisfactorily reproducible from sample to sample and from batch to batch. Indeed, randomly selected Si NW FETs showed well-constrained V_{th} and I_{on} behavior, with values of 4.26 ± 1.10 V and 0.66 ± 0.22 μA, respectively (Figure 8C, D). The good reproducibility of the Si NW FETs can be attributed to the uniform density, the good alignment, and the preferential distribution of the Si NWs. Figure 8E shows the average V_{th} of different Si NW FETs as a function of the channel width. **NOTE:** The densities of the sprayed Si NWs of all examined devices were similar to each other (1 NW/μm^2). As seen in the figure, the V_{th} showed a distribution that is not affected by the channel width, indicating that the V_{th} is not affected by the number of Si NWs connected between the source and drain electrodes. This could be

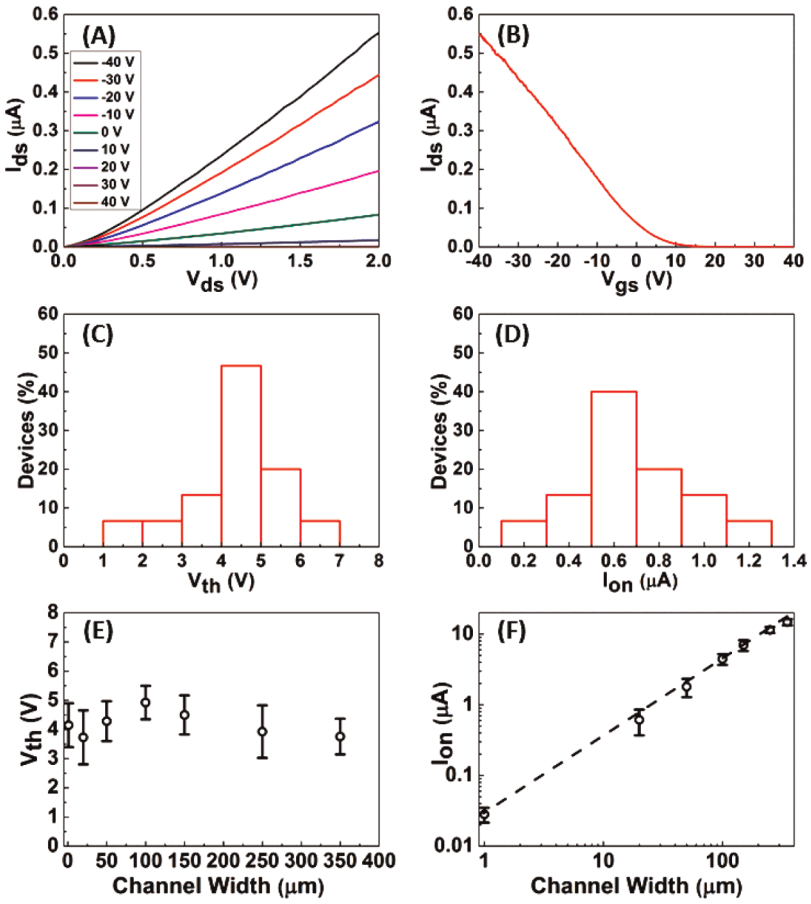

Figure 8. Devices based on spray-coated Si NW arrays with a density of ~1 NW/μm^2. (A) Family of source–drain current (I_{ds}) *versus* source–drain voltage (V_{ds}) plots at different gate voltages (V_{gs}); (B) I_{ds} *versus* gate V_g recorded for a typical device plotted on linear scales at V_{ds} = 2 V; (C) histogram of the threshold voltage (V_{th}) determined from analysis of 15 randomly chosen devices; (D) histogram of on-current (I_{on}) determined from analysis of 15 randomly chosen devices; (E) I_{on} as a function of the channel width; and (F) V_{th} as a function of the channel width.

attributed to hysteresis in the electrical characteristics of the Si NW FETs, probably due to variances in the surface states (such as dangling bonds, defects, and adsorbates) of the different Si NWs deposited on the substrate.[6,48,49] The average I_{on} of the Si NW FETs as a function of the channel width is shown in Figure 8F. It can be clearly seen that the I_{on} linearly scales with the channel width, with a slope of 0.04 μA/μm. Since a single Si NW in a back-gated geometry delivers ~0.04 μA (on average), the obtained 0.04 μA/μm slope in Figure 8F can correspond with 1 NW/μm. The highly linear scaling of the I_{on} with the channel width demonstrates the uniformity and reproducibility of the well-aligned NW arrays that are enabled through the reported spray-coating method.

DISCUSSION

The spray-coating route of a NW suspension uses a stream of fast moving nitrogen gas. We hypothesize that the high velocity of the nitrogen atomizes the NW suspension through the nozzle of the spray-coating gun and produces microscopic droplets. The dynamics of atomization is controlled by the combined action of viscous shear forces (due to a fast flow of the carrier gas) and capillary forces. The droplet size distribution is majorly controlled by the pressure/flow rate of the carrier gas. The droplets generated in the nozzle elongate in the direction of the fast gas flow due to the associated shear forces. At a certain gas flow rate (pressure), the size of the generated droplet becomes comparable to the length of a single NW (around 12 μm; see Figure 9A), and its shear-driven elongation (prior to pinching off) yields alignment of the confined NW in the spraying direction. The droplets with the encapsulated and flow-oriented NWs are accelerated toward the surface of the substrate *via* a stream of nitrogen and collide into the substrate. Considerable deformation/flattening of the droplets upon impact bring the confined NWs within the effective range of attractive intermolecular (van der Waals) forces, yielding their fast immobilization on the surface. Another plausible hypothesis is that the droplet elongation upon impact yields an alignment of the confined Si NWs in the spraying direction prior to their immobilization on the substrate. It is also possible that there is a

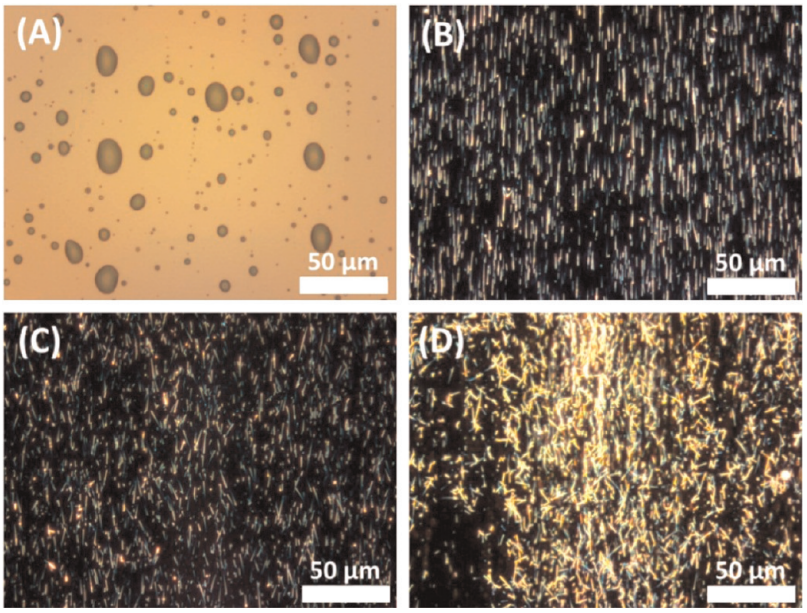

Figure 9. (A) Optical microscopy image of the droplets formed by the spray-coating process with a spray flow pressure of 40 psi. (B) Dark-field optical image of Si NWs formed *via* 12 ± 4 μm (sprayed) droplets. (C) Dark-field optical image of Si NWs formed *via* 50 ± 10 μm (sprayed) droplets. (D) Dark-field optical image of Si NWs formed *via* 300 ± 50 μm (sprayed) droplets. The spray-coating process was carried out on a SiO_x/Si receiver substrate with a spray flow pressure of 40 psi and on a receiver substrate at 75 °C.

secondary mechanism of alignment, where the NWs are not immobilized upon impact with the receiver substrate: the shear force exerted by the fast flow of the carrier gas over deposited droplets wetting the substrate results in their elongation and spreading in the spraying direction. The shear-induced elongation and possibly spreading of the deposited microdrops yields reorientation of the suspended Si NWs, resulting in their alignment in the flow direction before they are immobilized on the substrate due to solvent evaporation.

The increase in the pressure of the carrier gas yields an improved alignment. At a pressure above ~20 psi, >90% alignment was attained (see Figure 2). Since elevating the gas pressure yields smaller droplets, this finding indicates that at a pressure of ~20 psi a single NW is confined within a single droplet at most. Further increase in the gas pressure up to 60 psi may yield even smaller droplets, while the length of a single NW limits the size of the largest droplet encapsulating the NW, and therefore, the degree of alignment is not impaired.

The temperature is shown to have some effect on the quality of the NW alignment. At low temperatures of the receiver substrate (between 25 and 75 °C), a minor improvement in the alignment (~5%) was found upon increasing the temperature. Increasing the temperature above the solvent boiling point at ~82 °C affected the uniformity of the Si NW alignment adversely (see Figure 3). We argue that in the course of spray-coating microdroplets impact the prewetted substrate due to continuous droplet deposition and their shear-induced spreading. Increasing the temperatures up to 82 °C enhances solvent evaporation, yielding thinner solvent films and better interaction between the NW and the substrate upon impact. On the other hand, a receiver substrate that has temperatures above the solvent boiling point can cause solvent pops in the deposited film, adversely affecting the uniformity of the Si NW alignment. At high temperatures, well above the solvent boiling point (above ~200 °C), solvent evaporation is fast enough to keep the substrate dry, and some restoration of the alignment is observed (see Figure 3).

As long as separate small drops are deposited on the surface, the density of the Si NWs can be simply controlled by the duration of the flow, as shown in Figure 4. If the droplet produced at the nozzle is too large, *viz.*, encapsulating too many NWs, the alignment is deteriorated. A reduced concentration of NWs would lead to a lower surface coverage, as long as drops about the size of the NW are produced. High concentration of the NWs in the suspension may result in too many NWs confined in a single droplet, reducing the alignment. The effect of droplet size on the alignment and density of the deposited Si NW arrays in the spray-coating process was examined by controlling the size of the sprayed droplets (12 ± 4, 50 ± 10, and 300 ± 50 μm in diameter; see Figure 9B, C), *via* regulating the cross section of the nozzle's spray-coating gun. The results showed that droplet sizes with a mean diameter higher than 12 ± 4 μm adversely affect the uniformity of the Si NWs' alignment. In such cases, the Si NWs exhibited poor alignment with respect to

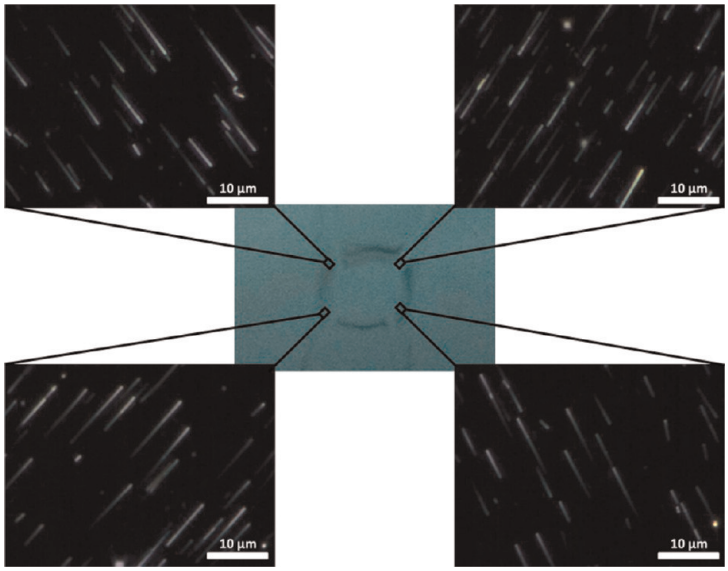

Figure 10. Spray-coating of Si NWs at a 90° angle between the spray gun and the receiver substrate. The experiment was carried out with an air pressure of 40 psi and on a receiver substrate at 75 °C.

the flow direction and were randomly aggregated on the surface, forming 3D (Si NW) islands (see Figure 9D). This observation could be attributed to a number of Si NWs embedded within a single droplet generated at the nozzle, leading to a reduced confinement and, as a result, to a lowered alignment in the spraying direction. It is worthwhile to point out in this context that the potential impact-driven elongation of a droplet that is considerably larger than a single NW should not affect the orientation of engulfed NWs, as the effect of confinement is lost.

To shed light on the transfer mechanism of Si NWs to the receiver substrate, spray-coating experiments were carried out at different angles between the spray gun and the receiver substrate in the range of 5° to 90°. The results showed that the alignment along one direction of the deposited Si NWs was affected, critically, by the angle between the nozzle and the receiver substrate. Increasing the angle between the spray gun and the receiver substrate in the range of 5° to 90° showed a high alignment, coherent with the flow direction in different regions of the substrate relative to the position of the gun. For example, spraying at a 90° angle between the spray gun and the receiver substrate showed a Si NW alignment in a large-scale radial pattern; see Figure 10. High alignment (86−91%) of the deposited Si NWs irrespective of the surface modification type (see Figures 5 and 7) indicates that the proposed spray-coating method is majorly insensitive to the wettability of the receiver substrate. Moreover, spray-coating the hydrophobic substrate using a Ag NW dispersion in water (see Supporting Information, Figure 2S) demonstrates unequivocally that immobilization/alignment occurs primarily upon impact and does not necessitate the shear-driven spreading/elongation of the deposited droplets; in this case the deposited (spherical) microdroplets slide along the surface without sticking to it and elongating in the flow direction. The dynamics of the droplet impact on the surface (and subsequent inertial elongation) and, as a result, the degree of alignment are, therefore, expected to be largely independent of the substrate type, chemistry, and wettability of the substrate.

SUMMARY AND CONCLUSIONS

We have shown that spray-coating of NWs suspension under controlled conditions of temperature, droplet size, spray-coating angle, and air flow is a successful method for preparing well-aligned and well-controlled Si NW, GaN NW, and Ag NW arrays. The quality and reproducibility of the spray-coated NW arrays were demonstrated by the production of highly uniform Si NW FETs. Complementary experiments indicated that the dynamics of droplet formation is understood by a combined action of viscous shear forces and capillary forces. Provided that the size of the deposited droplet is comparable to the length of the single NW, the shear-driven elongation of the generated droplets results presumably in the alignment of the confined NWs in the spraying direction. Flattening and possibly inertial elongation in the spraying direction of the microdroplets upon their impact onto the substrate yield fast immobilization of aligned NWs on the surface due to van der Waals attraction.

The transfer of highly aligned and controlled-density (Si) NWs to both large crystalline substrates and flexible plastic substrates provides important

advances toward achieving technological implementation of these materials in several areas of electronics and/or (bio)sensors. The availability of the spray-coating technique in current microelectronics technology would ensure immediate implementation in the production lines, with minimal changes in the fabrication design and/or auxiliary tools used for this purpose.

METHODS

The deposition method developed and tested in the current study is based on a spray-coating process under controlled conditions (Figure 1). The spray-coating system consisted of a hot plate for controlling the temperature of the receiver substrate, a pressure-flow spray nozzle module, a nozzle movement module, a nozzle angle control module, and a nozzle cross-section control module. Detailed information on each part of this process is provided in the following sections.

Preparation of NW Suspensions. The Si NWs investigated in this study were prepared by the vapor−liquid−solid (VLS) growth technique using gold nanoparticles as catalysts under a constant flow of 4 sccm silane, 5 sccm argon, and 1 sccm diborane (100 ppm in He), yielding p-type Si NWs.[50] Scanning electron microscopy data indicated that these Si NWs consisted almost entirely of a smooth crystalline core (40 ± 8 nm in diameter; see Figure 1A) with a length ranging between 8 and 13 μm. In a few cases, the Si NWs were etched with oxygen plasma (50 W) for 1 min. Immediately afterward, the Si NWs were transferred to a drybox with a nitrogen atmosphere for reaction with a ~5 mM chloroform-based or toluene-based solution of 3-aminopropyltrimethoxysilane (Sigma-Aldrich, Inc.), to form NH_2-terminated Si NWs, and with a solution of 2-perfluorooctylethyltrichlorosilane (ABCR, Inc.), to form CF_3-terminated Si NWs. After 45 min reaction time, the modified Si NWs were rinsed with chloroform (or toluene), acetone, and 2-propanol and, further, baked at 100 °C for 2 h to remove physically adsorbed solvent molecules on the molecularly modified Si NWs surface. Successful and repeatable functionalization of the Si NWs was verified using X-ray photon spectroscopy (XPS) (cf. refs 51−55 for more technical considerations during the XPS analysis of functionalized Si NWs). Finally, the Si NWs were suspended in 2-propanol using an ultrasonic bath for 5 s to obtain 12 μm length Si NWs and for 3 min to obtain 2 μm length Si NWs. In all experiments, a freshly prepared suspension was used in order to prevent the aggregation of Si NWs in solution.

The GaN NWs investigated in this study were prepared by the VLS growth technique with the catalyst-free approach. A GaN nucleation layer was deposited at 1200 °C for 4 s with a Ga:N ratio of 510:1. The GaN NWs were grown at 1150 °C for 1 h with a Ga:N flux ratio of 68:1. Prior to use, the GaN NWs were cleaned by a sequential rinse with acetone, methanol, and 2-propanol and dried by a stream of nitrogen.

The Ag NWs investigated in this study were produced *via* the polyol reduction of $AgNO_3$, in which ethylene glycol serves as the solvent and a precursor to the reducing agent.[56] In addition to the use of poly(vinyl pyrrolidone) as a stabilizer, copper(II) chloride was added to the reaction to reduce the amount of free Ag^+ during the formation of initial seeds and scavenge adsorbed oxygen from the surface of the seeds once formed. In doing so, Ag NWs were grown preferentially.[56]

Treatment of the Receiver Substrate. Receiver substrates that were used included SiO_x/Si(111), glass (Waldemar Knittel Glasbearbeitungs-GmbH. Inc.), polyethylene terephthalate (PET; Sigma-Aldrich, Inc.), and SiO_x/Si substrates with a predefined Ti/Au (20/200 nm) pattern (100 μm width × 200 μm length). Prior to use, all receiver substrates were cleaned by ultrasonic treatment in acetone, methanol, and 2-propanol and dried by a stream of nitrogen. The "receiver" substrates were further cleaned and etched using oxygen plasma (50 W) for 30 min. In a few cases, the SiO_x/Si receiver substrates were reacted with a ~5 mM chloroform-based or toluene-based solution of trichlorooctadecylsilane (Sigma-Aldrich, Inc.), to form the CH_3-terminated receiver SiO_x/Si substrate, a solution of 3-aminopropyltrimethoxysilane (Sigma-Aldrich, Inc.), to form the NH_2-terminated SiO_x/Si receiver substrate, and 2-perfluorooctylethyltrichlorosilane (ABCR, Inc.), to form the CF_3-terminated SiO_x/Si receiver substrate.[57,58] After 45 min reaction time, the molecularly modified substrates were cleaned using an ultrasonic bath and baked at 100 °C for 2 h. Successful and repeatable functionalization of SiO_x/Si substrates was verified using XPS and spectroscopic ellipsometry measurements; see Supporting Information.

Deposition of NWs on the Receiver Substrate. The deposition of the NWs on the receiver substrates started with the placement of the (modified) "receiver" substrate on a hot plate at 25−200 °C. Once the receiver substrate reached a specific predetermined temperature, the suspension of NWs was applied using a spray gun (Prona R2-F) at 5−60 psi carrier gas (nitrogen) pressure, with 5 ± 2° tilting angle relative to the "receiver" substrate. The nozzle tip was usually held at a distance of 1 cm from the substrate. Images of NWs after deposition were obtained by a scanning electron microscope (e-LiNE, Raith, Dortmund, Germany) and by an optical microscope (Olympus BX51RF-5) that is equipped with a camera (Olympus CAM-LC20-Bundle).

Field Effect Transistors Based on Spray-Coated Si NW Array. Field effect transistors that are based on Si NW arrays were fabricated on a 300 nm thermal oxide coated heavily doped p-type silicon wafer (<0.005 ohm-cm, silicon materials), using conventional lithography and lift-off processes. Prior to the device fabrication, the top SiO_x surface was cleaned by ultrasonic treatment in acetone, methanol, and 2-propanol and slightly etched using oxygen plasma (50 W; 1 min) for removing residues of organic contaminations. Interdigitated electrodes were defined using photolithography (Karl Suss MA6Mask Aligner) and Ti/Au (40/110 nm) on top of the sprayed Si NW array. The native oxide on the Si NWs under contact was etched by BHF for 5 s immediately before being loaded into the metal deposition system. The length of the electrodes was 5 μm, and the gap between the source and the drain electrodes was 2 μm. An Agilent B1500A semiconductor device analyzer was used for electrical measurements. To assess the electrical characteristics of Si NW field effect transistors, two modes of voltage-dependent back-gate measurements were performed. In the first mode, voltages between −40 and +40 V, in steps of 10 V, were applied to the degenerately doped silicon substrate. For each gate voltage, the current−voltage (I−V) characteristics were measured between the two electrodes, *i.e.*, between the drain and source, contacted by a micromanipulator, at a bias range between 0 and +2 V, in steps of 50 mV, under ambient conditions. In the second mode, voltages of 2 V were applied between the two electrodes, and the current−back gate voltage (I_{ds}−V_{ds}) measurements were carried out using a sweeping voltage from −40 upward to +40 V, in steps of 200 mV, under ambient conditions.

Conflict of Interest: The authors declare no competing financial interest.

Acknowledgment. Funding for the research leading to these results has been provided by the FP7-Health Program under the LCAOS (grant agreement no. 258868). We acknowledge Dr. Boaz Pokroy (Technion) for the use of advanced microscopes in his laboratory, Dr. Muhammad Bashouti (Max Planck Institute−Erlangen) for assistance, and Dr. Viatcheslav Berejnov (McMaster University) for fruitful discussions. H.H. is a Knight of the Order of Academic Palms.

Supporting Information Available: Optical image of spray-coated GaN NWs and Ag NWs from a 2-propanol suspension; optical image of spray-coated Ag NWs from a water suspension; and surface analysis of bare and molecularly terminated SiO_x/Si surfaces by X-ray photoelectron spectroscopy and by spectroscopic ellipsometry. This material is available free of charge *via* the Internet at http://pubs.acs.org.

REFERENCES AND NOTES

1. Hoffmann, S.; Bauer, J.; Ronning, C.; Stelzner, T.; Michler, J.; Ballif, C.; Sivakov, V.; Christiansen, S. H. Axial p-n Junctions Realized in Silicon Nanowires by Ion Implantation. *Nano Lett.* **2009**, *9*, 1341–1344.
2. Huang, Y.; Duan, X.; Cui, Y.; Lauhon, L. J.; Kim, K.; Lieber, C. M. Logic Gates and Computation from Assembled Nanowire Building Blocks. *Science* **2001**, *294*, 1313–1317.
3. Duan, X.; Huang, Y.; Cui, Y.; Wang, J.; Lieber, C. M. Indium Phosphide Nanowires as Building Blocks for Nanoscale Electronic and Optoelectronic Devices. *Nature* **2001**, *409*, 66–69.
4. Paska, Y.; Haick, H. Interactive Effect of Hysteresis and Surface Chemistry on Gated Silicon Nanowire Gas Sensors. *ACS Appl. Mater. Interf.* **2012**, DOI: 10.1021/am300288z.
5. Paska, Y.; Stelzner, T.; Assad, O.; Tisch, U.; Christiansen, S.; Haick, H. Molecular Gating of Silicon Nanowire Field-Effect Transistors with Nonpolar Analytes. *ACS Nano* **2012**, *6*, 335–345.
6. Paska, Y.; Stelzner, T.; Christiansen, S.; Haick, H. Enhanced Sensing of Nonpolar Volatile Organic Compounds by Silicon Nanowire Field Effect Transistors. *ACS Nano* **2011**, *5*, 5620–5626.
7. Bashouti, M. Y.; Tung, R. T.; Haick, H. Tuning Electrical Properties of Si Nanowire Field Effect Transistors by Molecular Engineering. *Small* **2009**, *5*, 2761–2769.
8. Haick, H.; Hurley, P. T.; Hochbaum, A. I.; Yang, P.; Lewis, N. S. Electrical Characteristics and Chemical Stability of Non-Oxidized, Methyl-Terminated Silicon Nanowires. *J. Am. Chem. Soc.* **2006**, *128*, 8990–8991.
9. Cui, Y.; Zhong, Z.; Wang, D.; Wang, W. U.; Lieber, C. M. High Performance Silicon Nanowire Field Effect Transistors. *Nano Lett.* **2003**, *3*, 149–152.
10. Lugstein, A.; Steinmair, M.; Steiger, A.; Kosina, H.; Bertagnolli, E. Anomalous Piezoresistance Effect in Ultrastrained Silicon Nanowires. *Nano Lett.* **2010**, *10*, 3204–3208.
11. Rurali, R.; Cartoixà, X.; Galvão, D. S. Large Electromechanical Response in Silicon Nanowires Predicted from First-Principles Electronic Structure Calculations. *Phys. Rev. B* **2008**, *77*, 073403.
12. Zhang, D. F.; Drissen, W.; Breguet, J. M.; Clavel, R.; Michler, J. A High-Sensitivity and Quasi-Linear Capacitive Sensor for Nanomechanical Testing Applications. *J. Micromech. Microeng.* **2009**, *19*, 075003.
13. Tisch, U.; Haick, H. Nanomaterials for Cross-Reactive Sensor Arrays. *MRS Bull.* **2010**, *35*, 797–803.
14. Avdic, A.; Lugstein, A.; Schondorfer, C.; Bertagnolli, E. Focused Ion Beam Generated Antimony Nanowires for Microscale pH Sensors. *Appl. Phys. Lett.* **2009**, *95*, 223106–3.
15. Zheng, G.; Patolsky, F.; Cui, Y.; Wang, W. U.; Lieber, C. M. Multiplexed Electrical Detection of Cancer Markers with Nanowire Sensor Arrays. *Nat. Biotechnol.* **2005**, *23*, 1294–1301.
16. Wang, W. U.; Chen, C.; Lin, K.; Fang, Y.; Lieber, C. M. Label-Free Detection of Small-Molecule Protein Interactions by Using Nanowire Nanosensors. *Proc. Natl. Acad. Sci.* **2005**, *102*, 3208–3212.
17. Fan, Z.; Lu, J. G. Gate-Refreshable Nanowire Chemical Sensors. *Appl. Phys. Lett.* **2005**, *86*, 123510–3.
18. Fan, Z.; Wang, D.; Chang, P. C.; Tseng, W. Y.; Lu, J. G. ZnO Nanowire Field-Effect Transistor and Oxygen Sensing Property. *Appl. Phys. Lett.* **2004**, *85*, 5923–5925.
19. Zhang, D.; Liu, Z.; Li, C.; Tang, T.; Liu, X.; Han, S.; Lei, B.; Zhou, C. Detection of NO_2 Down to ppb Levels Using Individual and Multiple In_2O_3 Nanowire Devices. *Nano Lett.* **2004**, *4*, 1919–1924.
20. Patolsky, F.; Zheng, G.; Hayden, O.; Lakadamyali, M.; Zhuang, X.; Lieber, C. M. Electrical Detection of Single Viruses. *Proc. Natl. Acad. Sci.* **2004**, *101*, 14017–14022.
21. Hahm, J.-I.; Lieber, C. M. Direct Ultrasensitive Electrical Detection of DNA and DNA Sequence Variations Using Nanowire Nanosensors. *Nano Lett.* **2003**, *4*, 51–54.
22. Qi, P.; Vermesh, O.; Grecu, M.; Javey, A.; Wang, Q.; Dai, H.; Peng, S.; Cho, K. J. Toward Large Arrays of Multiplex Functionalized Carbon Nanotube Sensors for Highly Sensitive and Selective Molecular Detection. *Nano Lett.* **2003**, *3*, 347–351.
23. Kong, J.; Franklin, N. R.; Zhou, C.; Chapline, M. G.; Peng, S.; Cho, K.; Dai, H. Nanotube Molecular Wires as Chemical Sensors. *Science* **2000**, *287*, 622–625.
24. Cui, Y.; Wei, Q.; Park, H.; Lieber, C. M. Nanowire Nanosensors for Highly Sensitive and Selective Detection of Biological and Chemical Species. *Science* **2001**, *293*, 1289–1292.
25. Wang, J.; Gudiksen, M. S.; Duan, X.; Cui, Y.; Lieber, C. M. Highly Polarized Photoluminescence and Photodetection from Single Indium Phosphide Nanowires. *Science* **2001**, *293*, 1455–1457.
26. Zhong, Z.; Qian, F.; Wang, D.; Lieber, C. M. Synthesis of p-type Gallium Nitride Nanowires for Electronic and Photonic Nanodevices. *Nano Lett.* **2003**, *3*, 343–346.
27. Qian, F.; Gradecàk, S.; Li, Y.; Wen, C. Y.; Lieber, C. M. Core/Multishell Nanowire Heterostructures as Multicolor, High-Efficiency Light-Emitting Diodes. *Nano Lett.* **2005**, *5*, 2287–2291.
28. Greytak, A. B.; Barrelet, C. J.; Li, Y.; Lieber, C. M. Semiconductor Nanowire Laser and Nanowire Waveguide Electro-Optic Modulators. *Appl. Phys. Lett.* **2005**, *87*, 151103–3.
29. Fan, Z.; Chang, P.; Lu, J. G.; Walter, E. C.; Penner, R. M.; Lin, C.; Lee, H. P. Photoluminescence and Polarized Photodetection of Single ZnO Nanowires. *Appl. Phys. Lett.* **2004**, *85*, 6128–6130.
30. Huang, Y.; Duan, X.; Lieber, C. M. Nanowires for Integrated Multicolor Nanophotonics. *Small* **2005**, *1*, 142–147.
31. Duan, X.; Niu, C.; Sahi, V.; Chen, J.; Parce, J. W.; Empedocles, S.; Goldman, J. L. High-Performance Thin-Film Transistors Using Semiconductor Nanowires and Nanoribbons. *Nature* **2003**, *425*, 274–278.
32. Huang, Y.; Duan, X.; Wei, Q.; Lieber, C. M. Directed Assembly of One-Dimensional Nanostructures into Functional Networks. *Science* **2001**, *291*, 630–633.
33. Jin, S.; Whang, D.; McAlpine, M. C.; Friedman, R. S.; Wu, Y.; Lieber, C. M. Scalable Interconnection and Integration of Nanowire Devices without Registration. *Nano Lett.* **2004**, *4*, 915–919.
34. Tao, A.; Kim, F.; Hess, C.; Goldberger, J.; He, R.; Sun, Y.; Xia, Y.; Yang, P. Langmuir-Blodgett Silver Nanowire Monolayers for Molecular Sensing Using Surface-Enhanced Raman Spectroscopy. *Nano Lett.* **2003**, *3*, 1229–1233.
35. Li, X.; Zhang, L.; Wang, X.; Shimoyama, I.; Sun, X.; Seo, W. S.; Dai, H. Langmuir-Blodgett Assembly of Densely Aligned Single-Walled Carbon Nanotubes from Bulk Materials. *J. Am. Chem. Soc.* **2007**, *129*, 4890–4891.
36. Yu, G.; Cao, A.; Lieber, C. M. Large-Area Blown Bubble Films of Aligned Nanowires and Carbon Nanotubes. *Nat. Nanotechnol.* **2007**, *2*, 372–377.
37. Smith, P. A.; Nordquist, C. D.; Jackson, T. N.; Mayer, T. S.; Martin, B. R.; Mbindyo, J.; Mallouk, T. E. Electric-Field Assisted Assembly and Alignment of Metallic Nanowires. *Appl. Phys. Lett.* **2000**, *77*, 1399–1401.
38. Dong, L.; Bush, J.; Chirayos, V.; Solanki, R.; Jiao, J.; Ono, Y.; Conley, J.; Ulrich, B. D. Dielectrophoretically Controlled Fabrication of Single-Crystal Nickel Silicide Nanowire Interconnects. *Nano Lett.* **2005**, *5*, 2112–2115.
39. Englander, O.; Christensen, D.; Kim, J.; Lin, L.; Morris, S. J. S. Electric-Field Assisted Growth and Self-Assembly of Intrinsic Silicon Nanowires. *Nano Lett.* **2005**, *5*, 705–708.
40. Javey, A.; Nam, S. W.; Friedman, R. S.; Yan, H.; Lieber, C. M. Layer-by-Layer Assembly of Nanowires for Three-Dimensional, Multifunctional Electronics. *Nano Lett.* **2007**, *7*, 773–777.
41. Fan, Z.; Ho, J. C.; Jacobson, Z. A.; Yerushalmi, R.; Alley, R. L.; Razavi, H.; Javey, A. Wafer-Scale Assembly of Highly Ordered Semiconductor Nanowire Arrays by Contact Printing. *Nano Lett.* **2007**, *8*, 20–25.
42. Takahashi, T.; Takei, K.; Ho, J. C.; Chueh, Y.; Fan, Z.; Javey, A. Monolayer Resist for Patterned Contact Printing of Aligned Nanowire Arrays. *J. Am. Chem. Soc.* **2009**, *131*, 2102–2103.

43. Yerushalmi, R.; Jacobson, Z. A.; Ho, J. C.; Fan, Z.; Javey, A. Large Scale, Highly Ordered Assembly of Nanowire Parallel Arrays by Differential Roll Printing. *Appl. Phys. Lett.* **2007**, *91*, 203104–3.
44. Heo, K.; Cho, E.; Yang, J.; Kim, M.; Lee, M.; Lee, B.; Kwon, S.; Lee, M.; Jo, M.; Choi, H.; *et al*. Large Scale Assembly of Silicon Nanowire Network-Based Devices Using Conventional Microfabrication Facilities. *Nano Lett.* **2008**, *8*, 4523–4527.
45. The slight differences in the average alignment on the different functionalized surfaces are within the experimental error.
46. The channel length is defined as the distance between source and drain.
47. Li, J.; Zhang, Y.; To, S.; You, L.; Sun, Y. Effect of Nanowire Number, Diameter, and Doping Density on Nano-FET Biosensor Sensitivity. *ACS Nano* **2011**, *5*, 6661–6668.
48. He, T.; Corley, D. A.; Lu, M.; Di Spigna, N. H.; He, J.; Nackashi, D. P.; Franzon, P. D.; Tour, J. M. Controllable Molecular Modulation of Conductivity in Silicon-Based Devices. *J. Am. Cem. Soc.* **2009**, *131*, 10023–10030.
49. Jie, J.; Zhang, W.; Peng, K.; Yuan, G.; Lee, C. S.; Lee, S.-T. Surface-Dominated Transport Properties of Silicon Nanowires. *Adv. Funct. Mater.* **2008**, *18*, 3251–3257.
50. Stelzner, T.; Andra, G.; Wendler, E.; Wesch, W.; Scholz, R.; Goesele, U.; Christiansen, S. Growth of Silicon Nanowires by Chemical Vapor Deposition on Gold Implanted Silicon Substrates. *Nanotechnology* **2006**, *17*, 2895–2898.
51. Puniredd, S. R.; Assad, O.; Stelzner, T.; Christiansen, S.; Haick, H. Catalyst-Free Functionalization for Versatile Modification of Nonoxidized Silicon Structures. *Langmuir* **2011**, *27*, 4764–4771.
52. Bashouti, M. Y.; Paska, Y.; Puniredd, S. R.; Stelzner, T.; Christiansen, S.; Haick, H. Silicon Nanowires Terminated with Methyl Functionalities Exhibit Stronger Si-C Bonds than Equivalent 2D Surfaces. *Phys. Chem. Chem. Phys.* **2009**, *11*, 3845–3848.
53. Bashouti, M. Y.; Stelzner, T.; Berger, A.; Christiansen, S.; Haick, H. Covalent Attachment of Alkyl Functionality to 50 nm Silicon Nanowires through Chlorination/Alkylation Process. *J. Phys. Chem. C* **2009**, *113*, 14823–14828.
54. Bashouti, M. Y.; Stelzner, T.; Berger, A.; Christiansen, S.; Haick, H. Chemical Passivation of Silicon Nanowires with C1-C6 Alkyl Chains through Covalent Si-C Bonds. *J. Phys. Chem. C* **2008**, *112*, 19168–19172.
55. Assad, O.; Puniredd, S. R.; Stelzner, T.; Christiansen, S.; Haick, H. Stable Scaffolds for Reacting Si Nanowires with Further Organic Functionalities while Preserving Si-C Passivation of Surface Sites. *J. Am. Chem. Soc.* **2008**, *130*, 17670–17671.
56. Korte, K. E.; Skrabalak, S. E.; Xia, Y. Rapid Synthesis of Silver Nanowires through a CuCl- or $CuCl_2$-Mediated Polyol Process. *J. Mater. Chem.* **2008**, *18*, 437–441.
57. Stenger, D. A.; Georger, J. H.; Dulcey, C. S.; Hickman, J. J.; Rudolph, A. S.; Nielsen, T. B.; McCort, S. M.; Calvert, J. M. Coplanar Molecular Assemblies of Amino- and Perfluorinated Alkylsilanes: Characterization and Geometric Definition of Mammalian Cell Adhesion and Growth. *J. Am. Chem. Soc.* **1992**, *114*, 8435–8442.
58. Wasserman, S. R.; Tao, Y. T.; Whitesides, G. M. Structure and Reactivity of Alkylsiloxane Monolayers Formed by Reaction of Alkyltrichlorosilanes on Silicon Substrates. *Langmuir* **1989**, *5*, 1074–1087.